RSC Advances

PAPER

View Article Online
View Journal | View Issue

Cite this: *RSC Adv.*, 2022, **12**, 29865

Comparative study of Hg(II) biosorption performance of xanthated and charred sugarcane bagasse from aqueous solutions

Puspa Lal Homagai,*[a] Mahesh Bhattarai,[a] K. M. Radhika,[a] Kedar Nath Ghimire,[b] Hari Paudyal*[b] and Ajaya Bhattarai *[c]

The main target of this study was to evaluate the efficiency of charred xanthated sugarcane bagasse (CXSB) and charred sugarcane bagasse (CSB) in the removal of Hg(II) ions from aqueous media. Batch experiments were performed to study the experimental parameters such as effects of pH, concentration, contact time and temperature. The adsorption velocity of Hg(II) onto CSB and CXSB was fast and reached equilibrium within 60 minutes. Isotherm and kinetic studies showed that Hg(II) uptake using both the biosorbents followed Langmuir isotherm and pseudo second order kinetics. The maximum adsorption capacity of Hg(II) at optimum pH 4.5 onto CSB and CXSB was found to be 125 mg g^{-1} and 333.34 mg g^{-1}, respectively. A negative value of $\Delta G°$ and positive $\Delta S°$ value (0.24 kJ mol^{-1} for CSB and 0.18 kJ mol^{-1} for CXSB) for both the biosorbents confirm the spontaneous nature of Hg(II) adsorption. A positive value of $\Delta H°$ (52.06 kJ mol^{-1} for CSB and 30.82 kJ mol^{-1} for CXSB) suggests the endothermic nature of biosorption. The investigated results shows that CXSB compared to CSB can be used as a low cost and environmentally benign bio-adsorbent for the removal of Hg(II) ions from aqueous solutions.

Received 22nd August 2022
Accepted 13th October 2022

DOI: 10.1039/d2ra05266k

rsc.li/rsc-advances

1 Introduction

Heavy metal pollution into the environment due to various human activities and rapid industrialization is a matter of global concern these days.[1] Mercury is the only liquid metal in existence and it is found everywhere in air, water and soil. Mercury is found as a trace element in all living organisms including humans. It is the most toxic metal out of the big three poisonous metals, the other two being cadmium and lead.[2] Mercury has been used to prepare different substances in our daily lives due to its specific properties. Some of them are mercury vapor lamps, thermometers, barometer's amalgams of dentistry and different medicines.[3] Different compounds of mercury such as mercurous chloride, mercuric chloride, mercuric oxide, mercuric iodide and mercuric sulphide are used in allopathic, Ayurvedic and homeopathic medicines.[4] Phenyl mercury acetate and ethyl mercury are used as fungicides and antiseptics.[5] Mercuric chloride is used as an active chemical in different cosmetic products such as skin lightening soaps and skin whitening creams.[6] In Nepal, gold is coated on the roof of the Pashupati Nath and Indreswor Mahadev Temple by traditional method using an amalgamation process. Global mercury emission from all sources is estimated at about 7000 metric tons per year.[7] In the last forty years, increases of mercury have been noticed.[8] Even very low exposure of mercury can precipitate various health problems like nausea, vomiting, diarrhea, abdominal pain, renal failure and even death within a week.[9] Mercury used wrongly can lead to severe damage to the DNA and neuron degeneration.[10] Inorganic mercury causes neurological disturbances and organic salt of methyl and ethyl mercury(II) poisoning causes renal disturbances.[11] Elemental Hg with rain or snow water finally reach lakes or streams and bacteria in soil and sediments converts Hg to methyl mercury.[12] It is then taken by tiny aquatic plants and animals and small fish eat this organism, big fish eat small fish and finally taken by birds and higher animals thus bioaccumulation takes place.

In Japan during 1950s, 600 people died due to mercury poison called Minamata disease, where the affected fish was taken by the people.[13] Abraham Lincoln took a medicine called "Blue Mass" contained significant amounts of mercury.[14] During 1971–72, 452 people died from the grain treated methyl mercury-based fungicide which was the largest Iraqi epidemic.[15]

An ingredient in the influenza vaccine called thiomersal (ethyl and phenyl mercuric salts) was banned by the American Academy of Pediatrics (AAP) in 1999 since it was implicated in autism and mental retardation.[16] As a result, its use is now being phased out and appropriate management is needed for already existing mercury related products.

[a]*Department of Chemistry, Amrit Campus, Tribhuvan University, Kathmandu, Nepal. E-mail: homagaipl@gmail.com*

[b]*Central Department of Chemistry, Tribhuvan University, Kathmandu, Nepal. E-mail: haripaudyal9@gmail.com*

[c]*Department of Chemistry, M.M.A.M.C., Tribhuvan University, Kathmandu, Nepal. E-mail: ajaya.bhattarai@mmamc.tu.edu.np*

Removal of heavy metals can be done by conventional methods which include physical and chemical process such as ion exchange, chemical precipitation, electrochemical technique, reverse osmosis and biosorption technique.[17] However, most of the methods have high operating cost and need for the disposal of remaining solid wastes.[18] Due to the advantages of economic feasibility and environmentally friendly behavior biosorption technique is regarded as the best technique for removing heavy metals.[19]

It was found that there are some works regarding to the low-cost bio-adsorbents like chitosan, fly ash, orange waste, tea waste and apple waste.[20–23] However, there is still need of developing selective adsorbents with suitable functional groups onto the polymer matrices. Sugarcane bagasse contains cellulose 46%, hemicelluloses 24.5%, lignin 19.95%, fat and waxes 3.5% and other elements 1.7%.[24] The polysaccharides found in sugar cane bagasse are biopolymers having many hydroxyl and phenolic groups that can be chemically modified to form new compounds with changed properties.[25,26] In this regards, locally available sugarcane bagasse will be considered for the chemical modification with the introduction of xanthate group onto its polymer analog.[27,28] According to the HSAB principle mercury metal thus interaction with soft group such as sulphur group is more favorable thus the selectivity of xanthate group for Hg(II) is high due to the presence of sulphur functional group.[29,30] The high affinity of mercury towards sulphur is crucial in developing methods for the functionalization of various materials with sulphur for Hg(II) abatement. The technique of biosorption is favourable for mercury removal from water over other conventional techniques such as ion exchange, solvent extraction, membrane separation, precipitation, *etc.*[31]

Modified date pits, low cost, minimal pretreatment steps and locally abundant agricultural waste materials were effectively employed as an adsorbent for remediating Hg(II) from aqueous media.[32] Nanoscience and technology were used to remove not only toxic mercury but also removal of carcinogenic dyes and other heavy metals. For example, poly(1-amino-5-chloroanthraquinone) (PACA) nanofibrils were applied as novel nano adsorbents for highly toxic mercury removal from aqueous solutions.[33] Bimetallic Fe–Zn nanoparticles were synthesized[34] which was used for high performance removal of carcinogenic dyes and Fe_3O_4 magnetic nanoparticles were used for the removal of Ni(II) from aqueous solutions.[35] Citric acid coated magnetic nanoparticles were used for the removal of Cd(II) ions from aqueous solution.[36] Fe_3O_4/humic acid magnetic nano-sorbents was prepared for the removal of carcinogenic dye from real water samples.[37] Using copper coordinated dithiooxamide metal–organic frameworks (Cu-DTO MOFs), tartrazine was removed from aqueous solutions.[38]

Activated carbon-doped magnetic nanocomposites were used for removal of toxic dyes from wastewater.[39] $SnFe_2O_4$@-activated carbon magnetic nanocomposite was used for the removal of crystal violet from aqueous solution.[40]

In the literature it was found that the adsorbent materials were prepared from sugarcane bagasse and modified with thermal treatment and chemical activation through activating agents ($ZnCl_2$ and H_3PO_4). The modified adsorbents were then used to remove mercury (Hg(II)) from aqueous solutions.[41] Batch biosorption experiments were performed to explore the influence of the kinetics, isotherm, and pH, on Hg(II) biosorption. The biosorption process was the best described by the pseudo-second-order kinetics model.[41]

Interestingly, biomass-derived adsorbents are more effective than commercial activated carbons.[37,42,43] For example, *Trapa bispinosa's* peel biomass is used as an effective, low-cost, and new adsorbent to remove lead(II) from aqueous solutions.[44] Rice bran biomass were used to remove nickel.[45,46] Biomass from NaOH-pretreated *Mangifera indica* leaves was found to have the highest absorption capability.[47] For the removal of lead from wastewater, *Azadirachta indica* (neem) leaves biomass was used.[48]

Novel thiol functionalized sugarcane bagasse (SB) was synthesized and structurally characterized by various techniques like scanning electron microscopy (SEM), energy dispersive X-ray (EDAX) and Fourier transform infrared (FTIR) spectroscopy. The biosorption properties of Hg^{2+} as a function of pH, contact time and initial metal concentration were characterized by cold vapor AAS.[49]

Our main aim is to study of the effectiveness of biomass-derived adsorbents as charred xanthated sugarcane bagasse (CXSB) and charred sugarcane bagasse (CSB). Thus, prepared biosorbents will be applied for the removal of mercury from contaminated water which is the new technique no one has done yet. To accomplish our objective, batch experiments were mostly conducted to investigate the effects of pH, concentration, contact time, and temperature. We detected the Hg(II) adsorption velocity onto CSB and CXSB. Isotherm and kinetic studies were also investigated. The promising results will lead to more research and applications of CXSB for wastewater treatment.

2 Experimental

2.1 Material and methods

The feed material, sugarcane bagasse (SB), employed in this study was collected from juice vender Ratna park, Kathmandu, Nepal. It was washed several times with distilled water to remove external dirt and water-soluble organics then it was dried in hot air oven at 70 °C for 4 hours. Dried sugarcane bagasse was grounded into fine particle using grinding machine and finally sieved to pass through 250 microns. The final powder obtained in this way is termed as raw sugarcane bagasse and abbreviated as RSB. The chemicals such as $Hg(NO_3)_2 \cdot H_2O$, HCl, NaOH, CS_2, H_2SO_4, standard solution of mercury (1000 mg L^{-1}) for AAS calibration employed in this study were purchased from Merk Chemical Co. Ltd., Germany. All the chemicals used in this study were of analytical grade and employed without further purification.

2.1.1 Preparation of adsorbate. The stock solutions (1000 mg L^{-1}) of mercuric nitrate monohydrate were prepared by dissolving appropriate amount of Hg $(NO_3)_2 \cdot H_2O$ in double distilled water. The pH of experimental solutions (25, 50, 100, 200, 300, and 500 mg L^{-1}) were adjusted by using hydrochloric acid and sodium hydroxide solutions. All the working solutions

Scheme 1 Synthetic route of CSB from RSB by charring.[2]

of desired concentrations were diluted using 0.1 M HNO_3 solution at the time of experiments.

2.1.2 Adsorbent preparation. Raw sugarcane bagasse (RSB) was modified by charring and xanthation process for the application in Hg(II) removal. For this, about 200 g of dried powder of RSB was taken in a bucket and conc. H_2SO_4 was added to it to make it completely black in color. Hence, the process is called charring process which after washing and drying termed as charred sugarcane bagasse (CSB). It is inferred that the ring opening reaction of cellulose occurred to produced ketonic groups[50] which is clearly observed in Scheme 1.

Moreover, to improve the selectivity for Hg(II), the CSB was then converted to CXSB as follows. For this, 20 g of CSB was placed in a beaker containing 100 mL of 15% NaOH followed by dropwise addition of 20 mL of carbon-disulphide (CS_2) which was then stirred continuously and kept for 48 hours for completion of xanthation reaction. Then the mixture was washed with distilled water till the pH of the washing water becomes neutral. After neutralization, it was filtered and sun dried then finally dried in an oven at 60 °C. The xanthated material obtained in this way is termed as charred xanthated sugarcane bagasse and abbreviated here forth as CXSB. It was placed in a desiccator using silica gel as a dehydrating agent to make free from moisture before use. The detailed of the xanthation mechanism is shown in Scheme 2.

2.1.3 Analysis of adsorbate and characterization techniques. Surface morphology of the RSB, CSB, Hg(II) loaded CSB, CXSB and Hg(II) loaded CXSB were imaged with scanning electron microscope (S-3000N, Hitachi, USA). Elemental analysis was done by using an energy dispersive X-ray spectrometer (LECO CHN-932, Canada). The pH of the solution was adjusted by using pH meter (HM-30R, TOA, Japan). Surface charge of the CSB and CXSB were determined by using zeta potential analyzer (Q.I. Nova 2200e, USA). The modifications of various functional groups of sugarcane bagasse by charring and xanthation reaction were investigated by using Fourier transform infrared (FTIR) spectra recorded using FTIR spectrometer (FT/IR-410, Jasco, USA). The concentration of Hg(II) before and after biosorption using both the biosorbents were determined by using Atomic Absorption Spectroscopy (AAS-240, Agilent, USA).

2.1.4 Batch wise study for biosorption of Hg(II). The batch biosorption studies were carried out in 100 mL Erlenmeyer flasks containing 25 mg of the adsorbent (CSB or CXSB) in 25 mL of Hg(II) solution at room temperature on a rotary shaker at the agitation speed of 180 rpm. The effect of pH on biosorption rate was investigated in a pH range of 1–7, which was maintained by the additions of 0.1 N HCl or 0.1 N NaOH at the beginning of the experiment using both the adsorbents. Kinetic studies were conducted by shaking the solid liquid mixture at the dosage of 1 g L^{-1} by varying contact time keeping other parameters constant. Similarly, is other test were conducted by changing the concentration of Hg(II) ion. The effect of adsorbent dosage was performed to investigate the ability of investigated CSB and CXSB to remove Hg(II) from trace concentration by changing adsorbent amount at their optimum pH. The thermodynamic investigation was done by evaluating the biosorption behavior of Hg(II) by varying the temperature. The amount of the Hg(II) adsorbed (mg) per unit mass of biosorbent (q) and percentage biosorption (% A) were obtained by using following mass balance equations:[51]

$$q = (C_0 - C_e) \times V/m \quad (1)$$

$$\% A = (C_0 - C_e)/C_0 \quad (2)$$

where, C_0 and C_e are initial and equilibrium metal ion concentration (mg L^{-1}), respectively. q is amount of metal ion adsorbed per gram of biomass(mg g^{-1}), V is volume of the reaction mixture in liter and m is dry weight of biosorbent in gram.

3 Results and discussion

3.1 Characterization of biosorbents

3.1.1 Determinations of carbon and sulphur in RSB, CSB and CXSB. Table 1 shows the determination of various elements in the samples of RSB, CSB and CXSB. It shows that carbon is the major component in all the samples. Evaluation of such a high amount of carbon in all the samples as major amount is due to the existence of various polysaccharides including cellulose, hemicellulose and other sugar molecules in RSB. In addition, amount of sulphur in CSB is higher than RSB which can be reasonably attributed due to partial sulphonation of sugarcane biopolymer with the aid of concentrated sulphuric acid. More importantly, sulphur amount was increased from 0.80% to 1.31% after xanthation reaction of CSB with CS_2 that

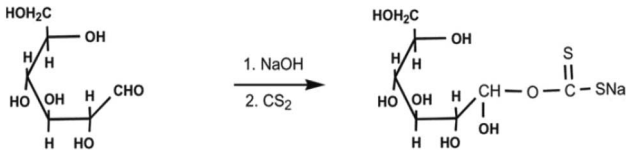

Scheme 2 Inferred mechanism for the xanthation of CSB to give CXSB.[2]

Table 1 Determination of carbon and sulphur in the sample of RSB, CSB and CXSB

S. No.	Samples	% C	% S
1	RSB	41.17	0.04
2	CSB	50.35	0.80
3	CXSB	44.68	1.31

clearly provides the evidence of effective incorporation of sulphur group onto polymer matrix of sugarcane bagasse *via* xanthation reaction as shown in Scheme 2.

3.1.2 Surface morphology analysis using FE-SEM technique. FE-SEM was used to observe the surface morphologies of RSB, CSB, Hg(II)–CSB, CXSB and Hg(II)–CXSB. To confirm the effect of the treatment on the samples were analyzed by scanning electron microscopy. The surface morphology of RSB, CSB, Hg(II) loaded CSB, CXSB and Hg(II) loaded CXSB were characterized by using FE-SEM (far emission scanning electron microscopy) images shown in Fig. 1a–e, respectively. It is clear from the results shown in FE-SEM image that the surface of RSB was found to be smooth whereas surface of CSB was relatively rough and non-uniform due to hydrolysis or sulphonation reaction on the surface of sugarcane bagasse by the action of concentrated sulphuric acid. It can be seen that the external surfaces of CXSB is full of cavities like a honeycomb structure. The xanthation reaction of CSB had considerably enhanced in the external morphology and its physical, chemical and biodegradable characteristics, which varies with respect to the nature of chemical modification. SEM observations of CSB revealed its non-uniform and rough surface that changed into irregular honeycomb structure of CXSB.

CXSB appeared to have isolated and irregularly distributed pores, which would be caused by the increase in the ineffective diffusion surface, which would help expose more surface-active binding sites and, ultimately, enhance the bagasse's biosorption capacity.

In case of Hg(II) adsorbed sample CXSB (Hg–CXSB) biosorption, the honeycomb surface like structure is completely filled and became much smooth surface which may be due to the incorporation of mercury which strongly indicates that the biosorption of Hg(II) takes place properly.

3.1.3 Evaluation of functional group modification by FTIR analysis. FTIR is a useful tool to identify the presence of certain functional groups in a molecule as each specific chemical bond of ten has a unique energy absorption band. The spectral analysis was employed to confirm changing of functional groups for pretreated and xanthated sugarcane bagasse. FTIR spectrum of the RSB, CSB, CXSB and Hg(II) adsorbed CXSB were recorded with KBr dispersion method by mixing biosorbent and KBr in 1 : 100 ratio and recorded the spectra as demonstrated in Fig. 2. The broad and intense absorption peaks observed at around 3442 cm^{-1} is due to the existence of bonded hydroxyl groups. The peaks observed at 2930 cm^{-1} can be assigned to the C–H group, and peaks around 1042 cm^{-1} is characteristics of C–O group of primary hydroxyls stretching that may be attributed to cellulose structure of the sugarcane bagasse. The band at 1754 cm^{-1} observed is due to stretching vibration of –CHO group that may be formed during the charring process *via* ring opening reaction as depicted in Scheme 1. This peak disappeared after modification of CSB into CXSB and a broad band depicted at 1558 cm^{-1} revealed that xanthate group has been introduced onto the CSB, which was confirmed from the increase of sulphur content of CSB after xanthation reaction. Absorption peaks appeared at 1558 cm^{-1} corresponding to the C=S stretching vibration of the xanthate unit and it may be attributed to the $-CS_2H$ deformation suggesting that CSB has been successfully xanthated and formed CXSB. The observation of peaks due to stretching vibration of C=S, S=O and S–S at 1176, 1022 and 460 cm^{-1}, respectively in the spectrum of CXSB are strong indicative of the presence of xanthate group bonded

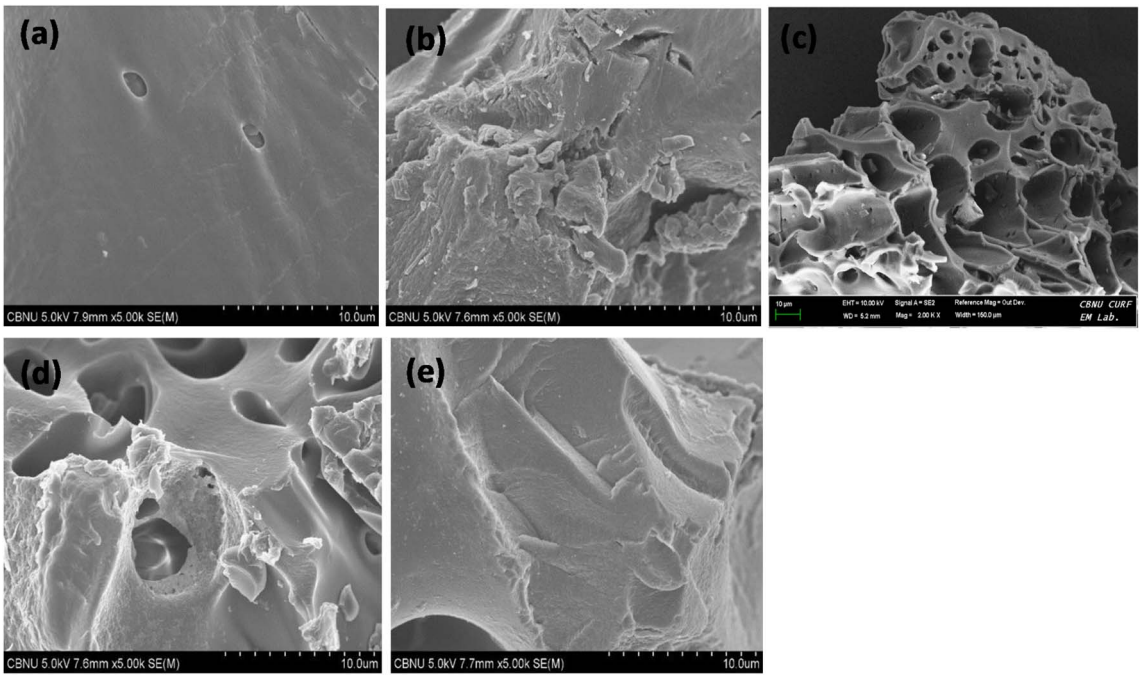

Fig. 1 SEM images of (a) RSB (b) CSB (c) Hg(II)–CSB (d) CXSB and (e) Hg(II)–CXSB.

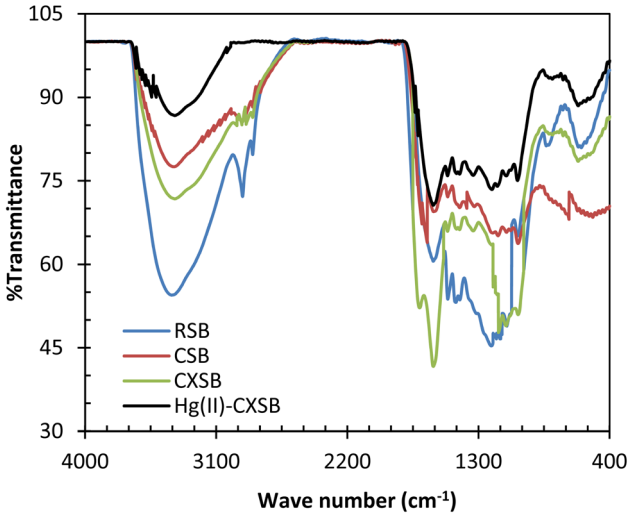

Fig. 2 FTIR images showing the surface morphologies of RSB, CSB, CXSB and Hg(II)–CXSB.

to the CSB. The major absorption bands corresponding to the characteristic of the C=S groups observed in the region at around 1563–700 cm^{-1}. This region is much more intense for CXSB in comparison to CSB. The peak corresponding to C–S–S and C–O–C symmetric stretching seemed to have merged into abroad band at 1558 cm^{-1}. The asymmetric stretching vibration of C–O–C is observed at 1176 cm^{-1}.[52]

The mechanism for the biosorption for the biosorption for heavy metals by sugarcane bagasse is linked to the role played by the essential stretching functional groups like hydroxyl (–OH), carboxylic (–COOH), carbonyl (C=O) and aromatic and phenolic groups. FTIR spectra provide fingerprints of vibration due to inter and intermolecular hydrogen bonding of polymeric compounds like alcohols, phenols and carboxylic acids as in cellulose, hemicelluloses and lignin, indicating the presence of free hydroxyl groups on the biosorbent surface. A sharp difference in FTIR spectra was noticed in CSB compared to RSB as shown in Fig. 2. The intense sharp peak at 3411 cm^{-1} in RSB has been shifted to 3429 cm^{-1} as a broad peak in CSB which is due to the overlapping of the hydroxyl group with amine group. This also suggests the introduction of amine group onto surface of biosorbent. The intense sharp peak at 1733 cm^{-1} in RSB has been shifted to 1705 cm^{-1} (C=O) as a broad peak in CSB. The peak at 1051 cm^{-1} in RSB has been shifted to 1172 (S=O) cm^{-1} CSB. The sharp difference in IR spectra was noticed in the surface modified charred sugarcane bagasse Hg(II)–CSB as shown in Fig. 2. In addition to this, the peak at 2918 cm^{-1} in RSB has been shifted to 2923 cm^{-1} (C–H) alkene group, and the peak at 1733 cm^{-1} (C=O) in RSB has been shifted to 1704 cm^{-1} (C=O) aldehyde group. The sharp peak at 1051 cm^{-1} in RSB has been shifted to 1202 cm^{-1} (C–O) tertiary alcohol in modified sugarcane bagasse which is due to the overlapping of the cyclic amide group with tertiary alcohol group. These provides the evidence that functional groups of RSB were modified by chairing and sulphur enriched functional groups were introduced during xantation process thereby enhance the Hg(II) biosorption.

3.1.4 Thermal analysis. Thermal analysis (TG) was performed to understand the stability characteristics of the charred sugarcane bagasse (CSB) cellulose and charred xanthated sugarcane bagasse (CXSB) cellulose, which is important during the processing of fibers into composites. The experiments were carried out under continuous N_2 atmosphere using a thermal analyzer with a heating rate of 10 °C min^{-1}. The charred sugarcane bagasse degraded mainly in two decomposition steps: the first at 250 °C and second one at 450 °C (Fig. 3a). Same way, CXSB also showed two decomposition steps at 300 °C and 810 °C (Fig. 3b) respectively. These results are depicted in the TGA and DTA curves shown in Fig. 3 for CSB and CXSB. The first stage started at about 100 °C for all the materials with weight loss of 10–20% due to loss of physically adsorbed water on membrane surfaces. The second stage exhibited a rapid weight loss at 250–450 °C and 300–810 °C for CSB and CXSB, respectively. The maximum oxidation reached at 450 °C for CSB and 810 °C for CXSB. The second degradation stage of CXSB took place at higher temperatures than the corresponding stage of CSB indicating that CSB is less stable than CXSB. The weight

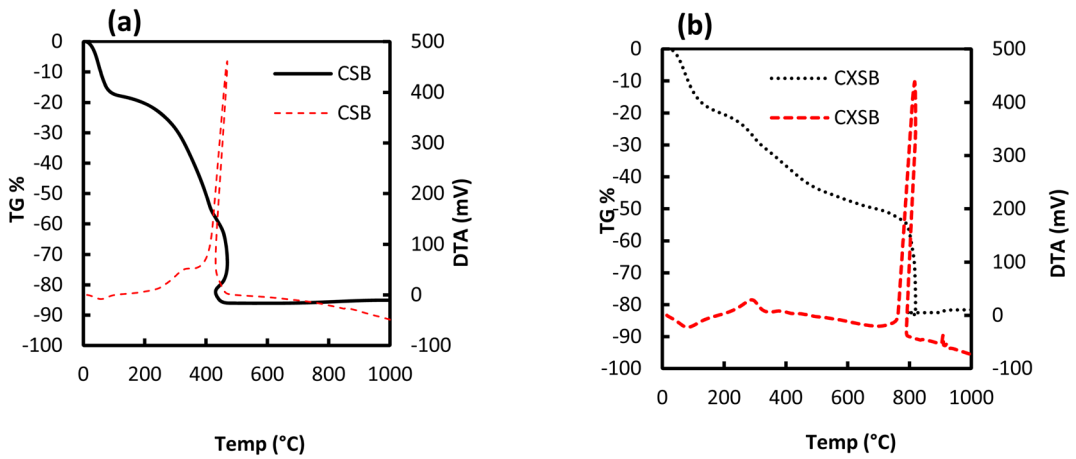

Fig. 3 Thermogravimetric (– TG) and differential thermogravimetric (--- DTG) curves for (a) CSB and (b) CXSB.

loss for CSB (250–450 °C) and CXSB (300–810 °C) were found to be about 90% and 80% respectively.

The DTA curves (Fig. 3a and b) revealed interesting and more accurate differences of the thermal behavior of the CSB and CXSB than the TGA curves. The DTA peak of CXSB had shown its maximum value at about 810 °C, while it is 450 °C for CSB indicating a strong evident in the increase in thermal stability of the CXSB over CSB. From the aforementioned analysis it is concluded that chemical modification has taken place within the CSB.

3.2 Influence of pH for the biosorption of Hg(II) ions

The pH of the Hg(II) solution is one of the controlling parameter during biosorption process. The surface charge of boisorbents and speciation of Hg(II) dramatically changes with pH variation. Effect of equilibrium pH on the removal of Hg(II) using CSB and CXSB is depicted in Fig. 4a. The results show that, the Hg(II) removal efficiency is lower at lower pH values for both the biosorbents whereas it is increased at higher pH using CXSB. The reason of increasing biosorption efficiencies of investigated biosorbent at elevated pH may be due to the cation exchange behavior. At strongly acidic pH, the biosorption efficiencies is low for both the biosorbents which is due to the competition of cationic species of Hg(II) ion with proton. From the comparative study of CSB and CXSB, the biosorption of Hg(II) by CSB occur at pH greater than 4 whereas CXSB occurred at wide range higher than 4.5. It is clear from the result of this figure that 62% removal of Hg(II) can be achieved by using CSB whereas it is more than 97% in case of CXSB.

The optimum pH of the solution can be explained on the basis of pHpzc (point of zero charge). The pHpzc is the pH at which the net charge of the adsorbent surface becomes zero. The point of zero charge for CSB and CXSB was found to be 7.5 and 4 respectively, as shown in Fig. 4b. Below pHpzc (pH < 4) the surface charge is positive and above pHpzc (pH > 4), the surface charge of the xanthated adsorbent is negative. Hence at more than pH 4, the sorption of the metal ions increased while the adsorption of metal ions decreases at pH less than 4. This signifies that the adsorption of metal ion takes place according to the ion exchange mechanism. The amount of adsorption above pHpzc was maximum due to the interaction of metal ions with a negatively charged adsorbent surface. At low pH, particularly below pHpzc, the positively charged metal ions and positively charged adsorbent surface species may repel with each other due to having an identical positive charge and thereby decreases the metal ion adsorption.[2] The result potentially reflected that there is high possibility of Hg(II) biosorption onto CXSB where surface of CXSB became gradually negative with increasing pH from 4 compared to CSB (it is 7.5 in CSB), resulting high percentage removal of Hg(II) by CXSB biosorbent than CSB. Therefore, the CXSB adsorbent investigated in this study can be a potential biosorbent for the treatment of aqueous solution polluted with Hg(II) ions.

3.3 Biosorption isotherms of Hg(II) ion

A biosorption isotherm provides the relationship between solid phase concentrations of adsorbate to the liquid phase concentrations. Adsorption capacity of RSB for Hg(II) removal was found to be 5 mg g^{-1} which is very low hence its further study was not done. Fig. 5a shows the results of Hg(II) uptake capacities of CSB and CXSB at different equilibrium concentration. It shows that the mercury uptake capacity of both the biosorbent increases at lower concentration areas of Hg(II) whereas it was found to be increase gradually and finally becomes nearly constant or plateau value at higher concentration of Hg(II) ion. This provides the characteristics of monolayer biosorption theory described by Langmuir in 1916. To investigate the best fitted isotherm model, the experimental data of concentration variation was modelled by using two well-known isotherms namely Langmuir and Freundlich isotherm models. Langmuir, Freundlich and Temkin models can be expressed in their linear form by using following relationships as:

$$\log q_e = \log K_F + (1/n)\log C_e \quad (3)$$

$$\frac{C_e}{q_e} = \frac{1}{q_{max}\, b} + \frac{1}{q_{max}} C_e \quad (4)$$

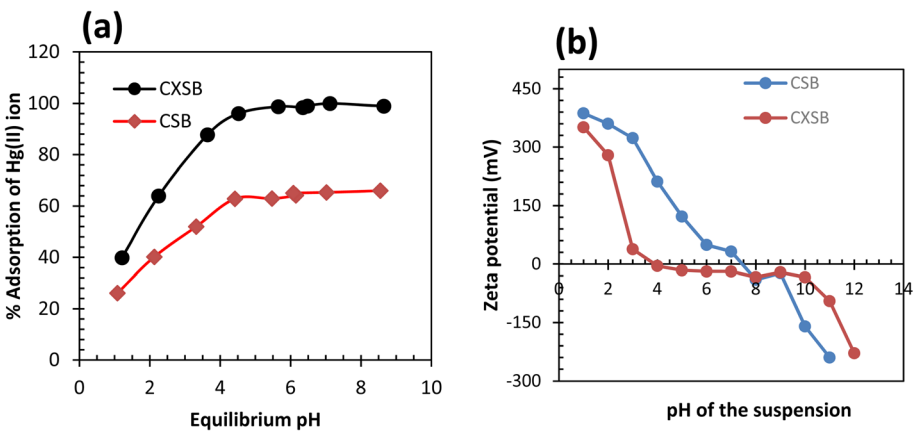

Fig. 4 Effect of pH onto CSB and CXSB (a) plot of *% A versus* pH (b) zeta potential of biosorbent-water suspension at different pH.

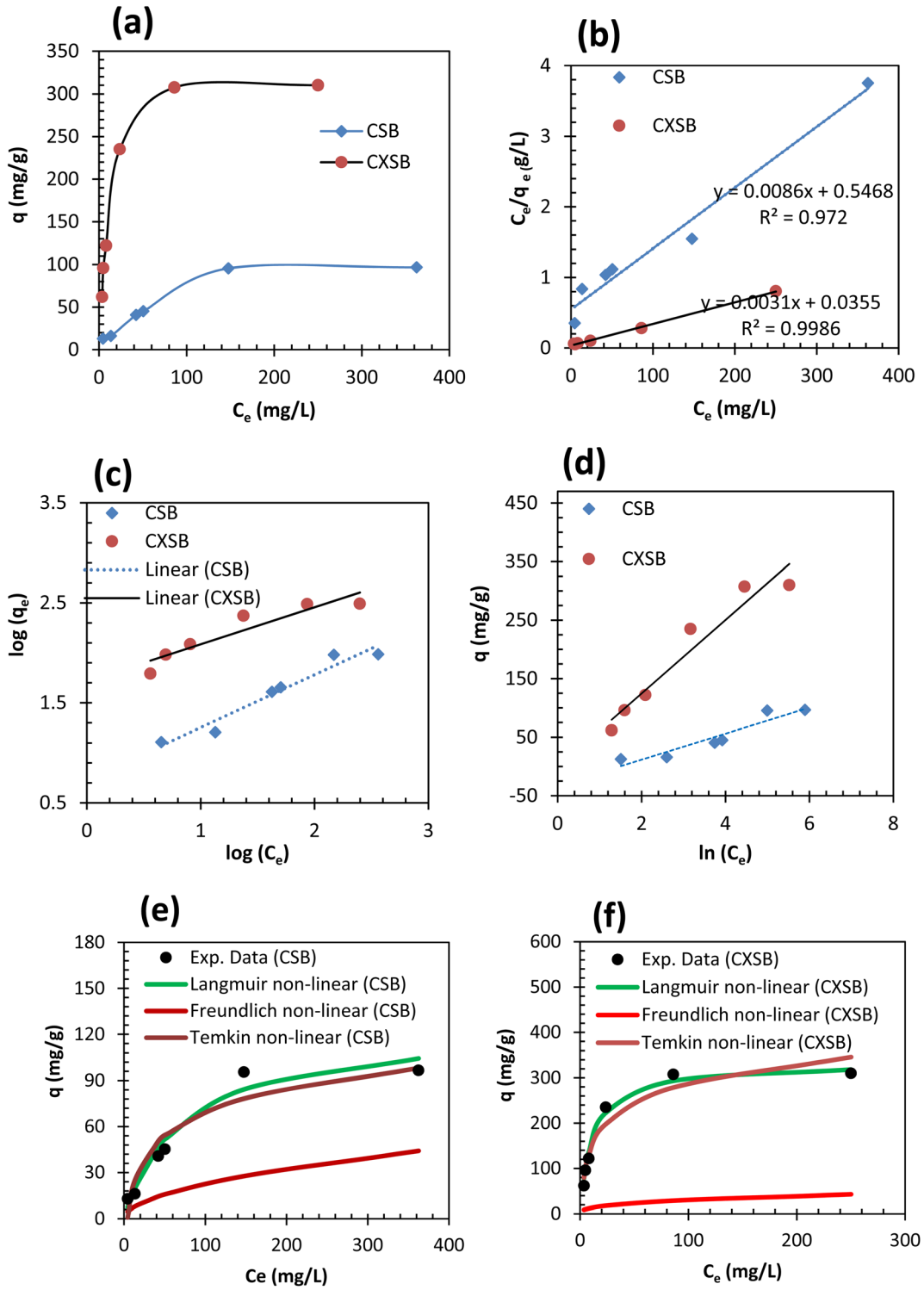

Fig. 5 Biosorption isotherm of Hg(II) using CSB and CXSB biosorbents (a) experimental isotherm plot, (b–d) linear plots of Langmuir, Freundlich and Temkin, (e and f) non-linear plots Langmuir, Freundlich and Temkin models.

$$q_e = B \ln A_T + B \ln C_e \quad \text{where,} \quad B = \frac{RT}{b_T} \tag{5}$$

where, C_e and q_e are the equilibrium concentration of Hg(II) and Hg(II) uptake by biosorbent at equilibrium, respectively. The constant b (L mg^{-1}) and q_{max} (mg g^{-1}) are Langmuir equilibrium parameter and maximum biosorption capacity. K_F and n are Freundlich constant related biosorption capacity and intensity respectively. Similarly, A_T and b_T are the Temkin constants. Langmuir parameters such as q_{max} and b were evaluated from the slope and intercept of the straight line obtained

Table 2 Langmuir and Freundlich parameters evaluated for the adsorption of Hg(II) onto CSB and CXSB

Isotherms models	Isotherm parameters	CSB	CXSB
Langmuir isotherm model	b (L mg^{-1})	0.014 ± 0.002	0.085 ± 0.007
	q_{max}, cal. (mg g^{-1})	125 ± 2.12	333.34 ± 5.47
	R^2	0.98	0.99
Freundlich isotherm model	K_F (mg g^{-1}) (mmol^{-1} min^{-1})	2.06 ± 0.14	5.56 ± 1.26
	$1/n$	0.52 ± 0.067	0.37 ± 0.018
	R^2	0.94	0.87
Temkin isotherm model	A_T	0.23 ± 0.036	0.98 ± 0.051
	b_T	111.60 ± 8.25	39.41 ± 0.96
	B	22.2 ± 1.58	62.87 ± 2.19
	R^2	0.89	0.93

by plotting C_e/q_e *versus* C_e (Fig. 5b), Freundlich isotherms parameters such as n and K_F were evaluated from the slope and intercept of $\log q_e$ *versus* $\log C_e$ (Fig. 5c), and Temkin isotherm parameters such as A_T and b_T were determined from the intercept and slope of q_e *versus* in (C_e) plot (Fig. 5d) and evaluated values are presented in Table 2. As can be seen from the results of this table that the correlation coefficients in case of Langmuir isotherm models is much higher and close to unity whereas its value is small in case of Freundlich isotherm model for both the adsorbents, indicating that Langmuir model is more suitable for the explanation of experimental data of Hg(II) adsorption. Moreover, the maximum Hg(II) adsorption capacities of CSB and CXSB were investigated to be 125 mg g^{-1} and 333.34 mg g^{-1}, respectively whereas that of Langmuir equilibrium constant (b) were found to be 0.014 and 0.085 for CSB and CXSB, respectively. For further confirmation, the Hg(II) uptake capacity of CSB and CXSB were determined by using non-linear Langmuir, Freundlich and Temkin equations and data are plotted together with experimental data as shown in figure Fig. 5e and f.

In both the case Hg(II) biosorption capacities evaluated from Langmuir isotherm model are closely resembled with experimental uptake capacity, providing strong evidence that biosorption of Hg(II) onto CSB and CXSB occurred according to Langmuir type monolayer adsorption theory.

Table 3 shows the comparative study of maximum Hg(II) sorption capacities of various adsorbents reported in the literature are presented together with CSB and CXSB investigated in this study. It shows that the sorbents such as algal biomass, carboxymethylated GAC, rice husk activated carbon, polyacrylate-modified carbon, sago waste-based AC and sugarcane bagasse washed with deionized water possess low biosorption capacity. On the other hand, the waste activated sludge, sulphur functionalized rice husk and investigated CSB and CXSB has high and comparable sorption potential, which suggest that the newly prepared CSB and CXSB biosorbents in this study can be potential materials for the treatment of Hg(II) ions from aqueous solution.

Table 3 Maximum Hg(II) uptake capacity of CSB and CXSB with other reported biosorbents

Adsorbents	q_{max} (mg g^{-1})	Reference
Activated carbon from rice husk (RHAC)	55.87	53
Algal biomass	42.00	54
Sulfur-functionalized rice straw (RSS)	119	55
Sulfur-functionalized rice husk (RHS)	92	56
Biopolymer from waste activated sludge	477	57
Unmodified granular activated carbon (GAC)	20.83	58
Carboxymethylated GAC	19.73	58
Polyacrylate-modified carbon	76.3	59
Sago waste-based AC	55.6	60
Sugarcane bagasse washed with deionized water	35.7	61
Charred sugarcane bagasse (CSB)	125	This study
Xanthated sugarcane bagasse (CXSB)	333.34	This study

3.4 Biosorption kinetics of Hg(II) ion

A series of contact time experiments for the biosorption of Hg(II) ions onto CSB and CXSB were carried out using 500 mg L^{-1} of Hg(II) ions at temperature 298.15, 308.15, and 318.15 K as shown in Fig. 6a biosorption. The result shows that the amount of biosorbed Hg(II) increased with an increase in contact time up to 120 min, after that there was no significant increase in the Hg(II) biosorption onto CSB (Fig. 6b) and CXSB (Fig. 6c).

In both the cases Hg(II) ions were rapidly adsorbed with increasing time at the beginnings and subsequently it become gradually slow until a steady state condition was attained at 2 h biosorption. Although biosorption equilibrium was attained in 2 h, subsequent biosorption experiment of Hg(II) removal were carried out by shaking the solid liquid mixture up to 24 h in order to ensure complete equilibrium.

To evaluate the best fitted kinetic models and plausible biosorption mechanism, the experimental data of Hg(II) biosorption were analyzed by pseudo first order (PFO), pseudo second order (PSO), and intra particle diffusion (IPD) models using the following equations.

PFO model

$$q_t = q_e(1 - e^{-k_1 t}) \quad (6)$$

$$\log(q_e - q_t) = \log q_e - \frac{k_1}{2.303} t \quad (7)$$

PSO model

$$q_t = \frac{k_2 q_e^2\, t}{1 + k_2 q_e\, t} \quad (8)$$

$$\frac{t}{q_t} = \frac{1}{k_2 q_e^2} + \frac{1}{q_e} t \quad (9)$$

Intra particle diffusion (IPD) model

$$q_t = k_{IPD} \times \sqrt{t} + C \quad (10)$$

where: q_e is the adsorption capacity at equilibrium (mg g^{-1}), q_t is the adsorption capacities at time t (mg g^{-1}), k_1 is the rate constant of first-order kinetic model (min^{-1}), t is the time of the

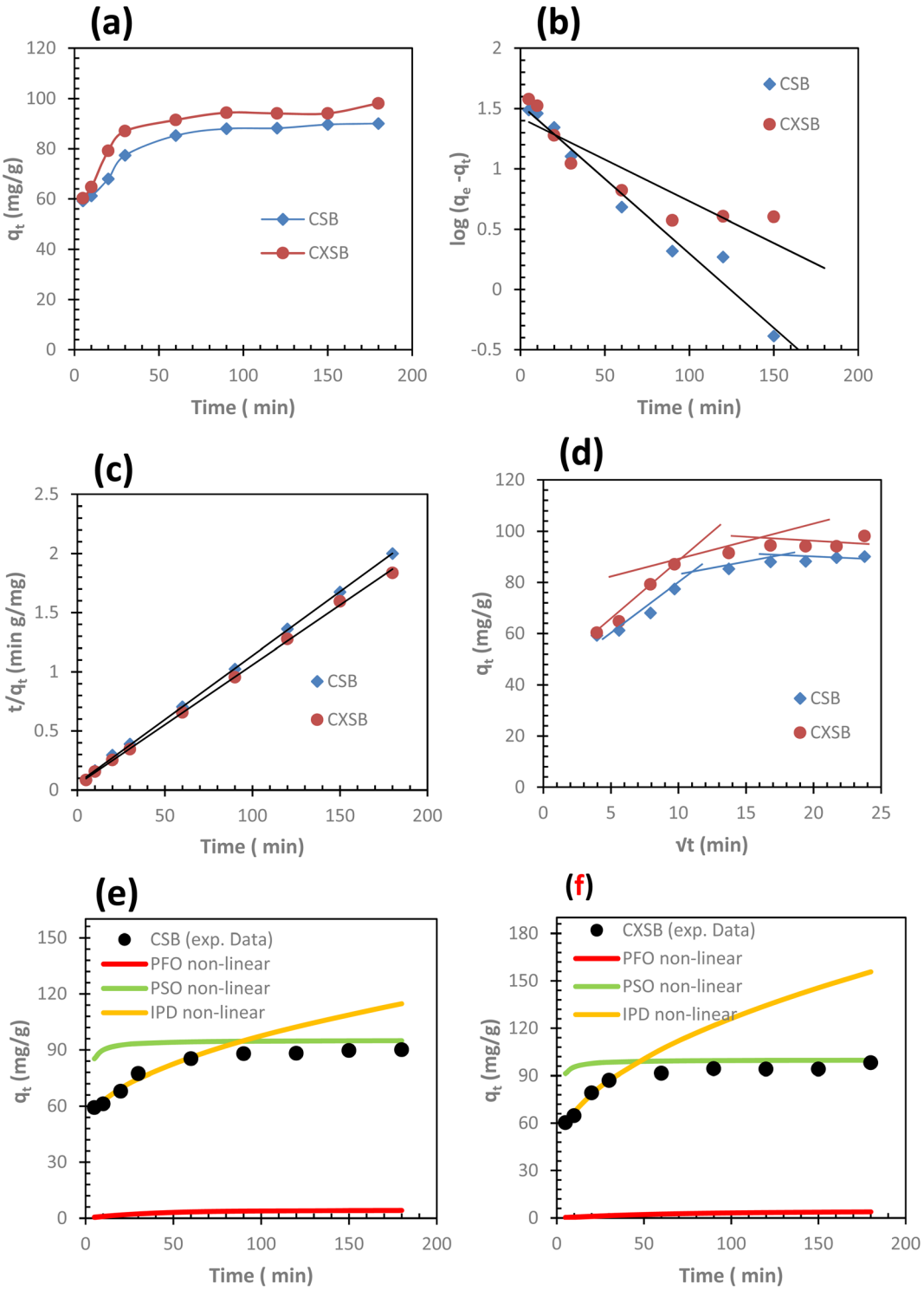

Fig. 6 Biosorption kinetics of Hg(II) onto CSB and CXSB (a) experimental plot, (b–d) linear fitting of kinetic data using PFO, PSO and IPD models, and (e and f) non-linear fitting of kinetic data using PFO, PSO and IPD models.

experiment (min), k_2 is the rate constant of the pseudo-second-order kinetic model (min^{-1}). k_{IPD} is the intraparticle diffusion rate constant (mg g^{-1} $min^{-1/2}$), and C is the plot's intercept of the Weber–Morris (W–M) diffusion model (mg g^{-1}).

The evaluated kinetic parameters of PFO, PSO and IPD for both CSB and CXSB are listed in Table 4 together with their correlation coefficients. From the results of this table, the experimental q_e value is very closed with the q_e calculated value determined from pseudo second order modeling compared to pseudo first order and intraparticle diffusion modeling for both the biosorbents. To further confirmation, the nonlinear modelling of kinetic data of Hg(II) biosorption for both the

Table 4 Kinetics parameters for the biosorption of Hg(II) onto CSB and CXSB

Kinetic models	Kinetic parameters	CSB	CXSB
Pseudo first order (PFO) model	k_1 (min^{-1})	0.027	0.014
	q_e, cal. (mg g^{-1})	4.13	4.15
	R^2	0.97	0.81
	q_e, exp. (mg g^{-1})	88.2	94.37
Pseudo second order (PSO) model	k_2 (g mg^{-1} min^{-1})	0.0018	0.0021
	q_e, cal. (mg g^{-1})	95.21	100.00
	R^2	0.99	0.99
	q_e, exp. (mg g^{-1})	88.2	94.37
Intra particle diffusion (IPD) model	k_{IPD} (mg min g^{-1})	2.85	4.88
	q_e, cal. (mg g^{-1})	39.88	46.81
	R^2	0.96	0.98

biosorbents were done using nonlinear equations of PFO, PSO and IPD and the result obtained for CSB and CXSB are presented in Fig. 6e and f, respectively. The result shows that Hg(II) uptake capacity of both CSB and CXSB evaluated using nonlinear modelling of PSO are more closely resembled with experimental data compared to PFO and IPD models. This clearly suggest that biosorption of Hg(II) onto investigated boisorbents follows pseudo second order kinetics.

3.5 Biosorption thermodynamics of Hg(II) ion using CSB and CXSB

The biosorption reactions are generally exothermic,[62] as the temperature increases, the percentage of biosorption decreases following the Le Chateliar's principle. At higher temperature the equilibrium constant for biosorption also decreases. These types of properties are found in case of physiosorption and change in enthalpy (ΔH°) will be negative. On the other hand, when percentage of biosorption increases with the increase of temperature giving the positive value of enthalpy change, then biosorption will be endothermic process. Such a phenomenon is mostly occurred in chemisorption process.

The equilibrium constant for the biosorption reaction can be determined using distribution coefficient at different temperature.[63]

$$K_D = \frac{C_i - C_e}{C_e} \times \frac{V}{m} = \frac{q_e}{C_e} \quad (11)$$

where, K_D is distribution coefficient and C_e is equilibrium concentration of Hg(II) ion in the solution. The distribution coefficient obtained from this equation has the unit of L g^{-1} thus it can be changed into dimensionless equilibrium constant by multiplying molarity of water (number of moles of pure water in one liter) and molecular weight of mercury. It can be expressed mathematically[64] as:

$$K_{equ} = K_D \times M_{water}\,(55.5) \times M_{Hg}\,(200.59) \quad (12)$$

The equilibrium constant is related to standard Gibbs free energy of the system as

$$\Delta G^\circ = -RT \ln K_{equ} \quad (13)$$

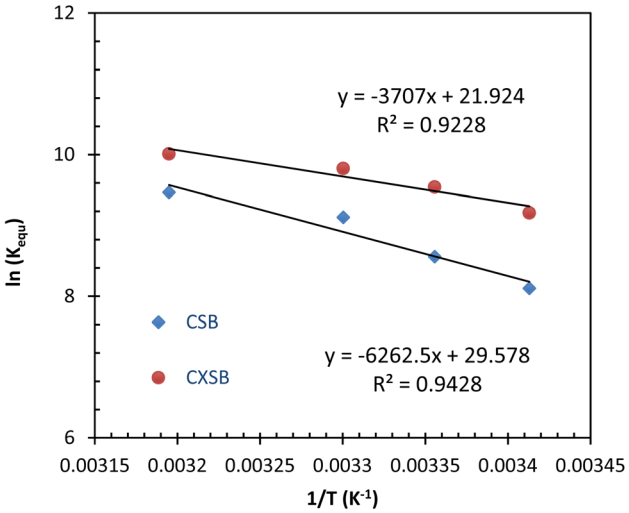

Fig. 7 Van't Hoff plots for the biosorption of Hg(II) using CSB and CXSB.

The relation between standard Gibb's free energy change, standard entropy change, and standard enthalpy change is as follows:

$$\Delta G^\circ = \Delta H^\circ - T\Delta S^\circ \quad (14)$$

Now equating eqn (13) and (14) we have

$$\ln(K_{equ}) = -\Delta H^\circ/RT + \Delta S^\circ/R \quad (15)$$

where, ΔG°, ΔH° and ΔS° are standard free energy change, standard enthalpy changes and standard entropy change, respectively. Van't Hoff plots for both CSB and CXSB are shown in Fig. 7. The ΔG° values were calculated directly by using eqn (8) whereas ΔH° and ΔS° for both the adsorbents were determined from the slope and intercept of the straight lines obtained from the Van't Hoff plots of $\ln K_{equ}$ *versus* $1/T$, respectively. These evaluated values are listed in Table 5. It shows that the value of ΔG° for both the adsorbents are negative for all the tested temperature indicating spontaneous nature of Hg(II) biosorption. Positive value of ΔH° (52.06 kJ mol^{-1} for CSB and 30.82 kJ mol^{-1} for CXSB) indicates that the adsorption process of mercury onto reported adsorbents is endothermic and positive ΔS° (0.24 kJ mol^{-1} for CSB and 0.18 kJ mol^{-1} for CXSB) values suggest spontaneous nature of biosorption and increase of disorderness near the interfacial region due to the release of some molecules or ions (here proton) during Hg(II) biosorption process. In addition, as the temperature increases, the ΔG° value decreases, and thus the adsorption process is energetically favorable at high temperatures.

3.6 Plausible adsorption mechanism

The probable mechanism between Hg–CXSB interaction could be electrostatic, ion exchange, and/or specific chemical reaction. The Hg(II) adsorption was found to be maximum at optimum pH and decreased in the pH range below the point of zero charge (pHpzc). The adsorption sites for Hg(II) are at sulfur

Table 5 Thermodynamic parameters determined for the sorption of Hg(II) onto CSB and CXSB

Adsorbent	T (K^{-1})	K_{equ}	$\ln(K_{equ})$	$\Delta G°$ (kJ mol^{-1})	$\Delta H°$ (kJ mol^{-1})	$\Delta S°$ (kJ mol^{-1} K^{-1})
CSB	293	3660.44	8.21	−19.98	52.06	0.24
	298	5254.55	8.55	−21.20		
	303	9082.09	9.11	−22.95		
	313	12 912.87	9.46	−24.63		
CXSB	293	9674.35	9.17	−26.04	30.82	0.18
	298	13 908.14	9.54	−24.69		
	303	18 055.09	9.80	−23.63		
	313	22 213.17	10.00	−26.04		

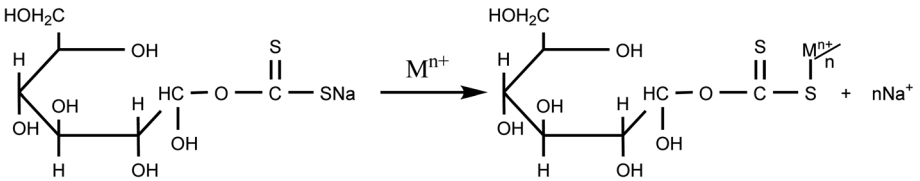

Scheme 3 Plausible adsorption mechanism of M^{n+}(Hg) ion onto monomeric cellulose unit contained in CXSB.[2]

atoms attached to the xanthate groups. The xanthate groups are unprotonated above pH 1.5 and have a net negative charge and hence the adsorption of Hg(II) with CXSB started above pH 2. Since the CXSB has a very low specific surface area (25 m^2 g^{-1}), physical adsorption alone cannot contribute to the higher Hg(II) ion uptake capacity, so the predominant mode of adsorption is the chemisorption. The cation from the xanthate group contained in the monomeric unit has been exchanged at the cost of Hg(II) ions present in the solution. A schematic representation of the complexation mechanism of the Hg(II) ions with the xanthate group which had taken place through the ion exchange process,[2] is shown in Scheme 3. According to the HSAB theory by Pearson, xanthate is a soft base and it tends to form stable complexes with soft acids like heavy metal ion *i.e.* Hg(II).[65] The metal such as Hg(II) are larger and more polarizable and the ligands, charred xanthated sugarcane bagasse will have a much higher affinity towards the Hg(II) ions and the sorption capacity was found to be higher than its charred biomass.

4 Conclusions

In summary, the novel types of biosorbent namely CSB and CXSB were prepared from locally available biowaste of sugarcane bagasse by simple sulphuric acid charring and xanthation reaction. Hg(II) removal efficiency of RSB improved after modification due to generation of more active adsorption sites. The CXSB can adsorb 98% Hg(II) from aqueous solution at optimum pH whereas CSB removes only 62% of Hg(II) under similar experimental conditions. Langmuir isotherm and pseudo second order kinetic model suitably describe the experimental data of Hg(II) adsorption. Maximum adsorption capacities of CSB and CXSB for Hg(II) ion were evaluated to be 125 mg g^{-1} and 333.34 mg g^{-1}, respectively. Negative value of $\Delta G°$ and positive value of $\Delta S°$ for both the biosorbents in all the tested temperatures confirms the spontaneous nature of Hg(II) adsorption. The positive value of $\Delta H°$ for both the biosorbent suggests the endothermic nature of adsorption reactions. The promising results of CXSB can be used as low cost and environmentally benign adsorbent for fast removal of Hg(II) from contaminated water. However, more investigations are recommended to study the stability and reusability of CXSB under pilot plant and industrial conditions.

Data availability

The data used in the present study are available from the corresponding authors upon reasonable request.

Author contributions

Kedar Nath Ghimire and Puspa Lal Homagai conceived and designed the experiments. Mahesh Bhattarai and KM Radhika performed the experiments and analyzed and interpreted the data. Puspa Lal Homagai contributed reagents, materials, analysis tools or data. Puspa Lal Homagai, Hari Paudyal and Ajaya Bhattarai wrote the paper.

Conflicts of interest

The authors declare that they have no conflict of interest.

Acknowledgements

The authors would like to thank Dr Deval Prasad Bhattarai, Chonbuk National University (CBNU), South Korea for the cooperation to do some characterizations of the bioadsorbents.

References

1 H. Ali, E. Khan and I. Ilahi, *J. Chem.*, 2019, **2019**, 1–14.

2 P. L. Homagai, K. N. Ghimire and K. Inoue, *Sep. Sci. Technol.*, 2010, **46**, 330–339.
3 J.-D. Park and W. Zheng, *Journal of Preventive Medicine and Public Health*, 2012, **45**, 344–352.
4 W. Sneader, *Drug Discovery. A History*, John Wiley & Sons Ltd, 2005.
5 WHO, *International Agency for Research on Cancer IAC Monograhs on Evaluation of Carcinogenic Risks to Humans, Beryllium, Cadmium, Mercury, and Exposures in the Glass Manufacturing Industry*, Lyon, 1993, vol. 58, pp. 9–16.
6 O. E. Dadzie and A. Petit, *J. Eur. Acad. Dermatol. Venereol.*, 2009, **23**, 741–750.
7 B. Gworek, W. Dmuchowski, A. H. Baczewska, P. Brągoszewska, O. Bemowska-Kałabun and J. Wrzosek-Jakubowska, *Water, Air, Soil Pollut.*, 2017, **228**, 123.
8 S. Cinnirella, D. E. Bruno, N. Pirrone, M. Horvat, I. Živković, D. C. Evers, S. Johnson and E. M. Sunderland, *Sci. Data*, 2019, **6**, 205.
9 K. M. Rice, E. M. Walker, M. Wu, C. Gillette and E. R. Blough, *Journal of Preventive Medicine and Public Health*, 2014, **47**, 74–83.
10 S. Jadoon and A. Malik, *Biochem. Pharmacol.*, 2018, **07**, 246.
11 R. A. Bernhoft, *J. Environ. Public Health*, 2012, **2012**, 1–10.
12 H. Hsu-Kim, C. S. Eckley, D. Achá, X. Feng, C. C. Gilmour, S. Jonsson and C. P. J. Mitchell, *Ambio*, 2018, **47**, 141–169.
13 N. Hachiya, Epidemiological Update of Methylmercury and Minamata Disease, in *Methylmercury and Neurotoxicity*, Springer US, 2012, pp. 1–11.
14 N. Hirschhorn, R. G. Feldman and I. Greaves, *Perspect. Biol. Med.*, 2001, **44**, 315–332.
15 S. B. Skerfving and J. F. Copplestone, *Bull. W. H. O.*, 1976, **54**, 101–112.
16 P. G. King and G. S. Goldman, *Med. Veritas*, 2008, **5**, 1610–1644.
17 N. A. Renu, M. Agarwal and K. Singh, *Interdiscipl. Environ. Rev.*, 2017, **18**, 124.
18 A. Tripathi and M. R. Ranjan, *J. Biorem. Biodegrad.*, 2015, **06**, 315.
19 M. Gavrilescu, *Eng. Life Sci.*, 2004, **4**, 219–232.
20 V. K. Gupta, P. J. M. Carrott, M. M. L. Ribeiro Carrott and Suhas, *Crit. Rev. Environ. Sci. Technol.*, 2009, **39**(10), 783–842.
21 C. K. Jain, D. S. Malik and A. K. Yadav, *Environ. Processes*, 2016, **3**, 495–523.
22 A. Malakahmad, S. Tan and S. Yavari, *J. Chem.*, 2016, **2016**, 1–8.
23 S. Singh, I. J. Chaudhary and P. Kumar, *International Journal of Scientific Research in Biological Sciences*, 2019, **6**, 56–61.
24 L. J. Maschio, P. H. F. Pereira and M. L. C. P. da Silva, *Carbohydr. Polym.*, 2012, **89**, 992–996.
25 G. Samchetshabam, S. P. Shukla, J. Matolia, C. Prakash, V. Bharti and A. R. Singh, *Global Challenges*, 2018, **2**, 1700131.
26 M. S. Nazir, Z. Tahir, M. N. Akhtar and M. A. Abdullah, *Applications of Ion Exchange Materials in the Environment*, 2019, pp. 135–159.
27 S. A. Ahmed, A. M. El-Roudi and A. A. A. Salem, *J. Environ. Sci. Technol.*, 2015, **8**, 338–351.
28 R. Khalilnezhad, M. E. Olya, M. Khosravi and R. Marandi, *Appl. Biochem. Biotechnol.*, 2014, **174**, 1919–1934.
29 S.-T. Song, N. Saman, K. Johari and H. Mat, *Environ. Prog. Sustainable Energy*, 2015, **34**, 1298–1310.
30 C. A. Prestidge, J. Ralston, R. St and C. Smart, *Colloids Surf., A*, 1993, **81**, 103–119.
31 T. Velempini and K. Pillay, *J. Environ. Chem. Eng.*, 2019, **7**, 103350.
32 M. A. Al-Ghouti, D. Da'ana, M. Abu-Dieyeh and M. Khraisheh, *Sci. Rep.*, 2019, **9**, 15327.
33 S. Huang, C. Ma, Y. Liao, C. Min, P. Du and Y. Jiang, *J. Nanomater.*, 2016, **2016**, 1–11.
34 R. K. Gautam, V. Rawat, S. Banerjee, M. A. Sanroman, S. Soni, S. K. Singh and M. C. Chattopadhyaya, *J. Mol. Liq.*, 2015, **212**, 227–236.
35 R. K. Gautam, P. K. Gautam, S. Banerjee, S. Soni, S. K. Singh and M. C. Chattopadhyaya, *J. Mol. Liq.*, 2015, **204**, 60–69.
36 D. Singh, R. K. Gautam, R. Kumar, B. K. Shukla, V. Shankar and V. Krishna, *J. Water Proc. Eng.*, 2014, **4**, 233–241.
37 R. K. Gautam and I. Tiwari, *Chemosphere*, 2020, **245**, 125553.
38 R. K. Gautam, S. Banerjee, M. A. Sanroman and M. C. Chattopadhyaya, *J. Environ. Chem. Eng.*, 2017, **5**, 328–340.
39 R. K. Gautam, N. Jaiswal, A. K. Singh and I. Tiwari, *Environ. Sci. Pollut. Res.*, 2021, **28**, 36680–36694.
40 P. Rai, R. K. Gautam, S. Banerjee, V. Rawat and M. C. Chattopadhyaya, *J. Environ. Chem. Eng.*, 2015, **3**, 2281–2291.
41 S. Giraldo, I. Robles, A. Ramirez, E. Flórez and N. Acelas, *SN Appl. Sci.*, 2020, **2**, 1029.
42 R. K. Gautam, A. Mudhoo, G. Lofrano and M. C. Chattopadhyaya, *J. Environ. Chem. Eng.*, 2014, **2**, 239–259.
43 R. K. Gautam, P. K. Gautam, S. Banerjee, V. Rawat, S. Soni, S. K. Sharma and M. C. Chattopadhyaya, *J. Environ. Chem. Eng.*, 2015, **3**, 79–88.
44 M. N. Zafar, M. Saeed, R. Nadeem, S. H. Sumrra, S. S. Shafqat and M. A. Qayyum, *Open Chem.*, 2019, **17**, 325–336.
45 M. N. Zafar, I. Aslam, R. Nadeem, S. Munir, U. A. Rana and S. U.-D. Khan, *J. Taiwan Inst. Chem. Eng.*, 2015, **46**, 82–88.
46 M. N. Zafar, I. Abbas, R. Nadeem, M. A. Sheikh and M. A. Ghauri, *Water, Air, Soil Pollut.*, 2008, **197**, 361–370.
47 R. Nadeem, M. N. Zafar, A. Afzal, M. A. Hanif and R. Saeed, *J. Taiwan Inst. Chem. Eng.*, 2014, **45**, 967–972.
48 M. N. Zafar, A. Parveen and R. Nadeem, *Desalin. Water Treat.*, 2013, **51**, 4459–4466.
49 A. Gupta, S. R. Vidyarthi and N. Sankararamakrishnan, *J. Environ. Chem. Eng.*, 2014, **2**, 1378–1385.
50 P. L. Homagai, K. N. Ghimire and K. Inoue, *Bioresour. Technol.*, 2010, **101**, 2067–2069.
51 S. E. Bailey, T. J. Olin, R. M. Bricka and D. D. Adrian, *Water Res.*, 1999, **33**, 2469–2479.
52 Silverstein, F. X. Webster and D. J. Kiemle, *Spectrometric Identification of Organic Compounds*, John Wiley and Sons, Hoboken, NJ, 7th edn, 2005.
53 M. Aslam, S. Rais, M. Alam and A. Pugazhendi, *J. Chem.*, 2013, **2013**, 1–11.

54 Z. Liu, Y. Sun, X. Xu, J. Qu and B. Qu, *ACS Omega*, 2020, **5**, 29231–29242.
55 M. Kumar, A. K. Singh and M. Sikandar, *Heliyon*, 2020, **6**, e03321.
56 M. Aslam, S. Rais, M. Alam and A. Pugazhendi, *J. Chem.*, 2013, **2013**, 1–11.
57 J. Zhang, P. Wang, Z. Zhang, P. Xiang and S. Xia, *Int. J. Environ. Res. Public Health*, 2020, **17**, 1488.
58 F. K. Onwu, *Am. J. Phys. Chem.*, 2014, **3**, 89–95.
59 M. Al-Yaari and T. A. Saleh, *ACS Omega*, 2022, **7**, 14820–14831.
60 K. Kadirvelu, M. Kavipriya, C. Karthika, N. Vennilamani and S. Pattabhi, *Carbon*, 2004, **42**, 745–752.
61 E. Khoramzadeh, B. Nasernejad and R. Halladj, *J. Taiwan Inst. Chem. Eng.*, 2013, **44**, 266–269.
62 I. Vishan, B. Saha, S. Sivaprakasam and A. Kalamdhad, *Environ. Technol. Innovation*, 2019, **14**, 100323.
63 M. Chiban, G. Carja, G. Lehutu and F. Sinan, *Arabian J. Chem.*, 2016, **9**, S988–S999.
64 E. C. Lima, A. Hosseini-Bandegharaei, J. C. Moreno-Piraján and I. Anastopoulos, *J. Mol. Liq.*, 2019, **273**, 425–434.
65 M. J. Winter, in *d-Block Chemistry*, Oxford University Press, New York, 1994.